MIT Open Access Articles

Edge turbulence measurements in L-mode and I-mode at ASDEX Upgrade

Edge turbulence measurements in L-mode and I-mode at ASDEX Upgrade

R. Bielajew, G. D. Conway, M. Griener, et al.

COLLECTIONS

Paper published as part of the special topic on Papers from the 63rd Annual Meeting of the APS Division of Plasma Physics

ARTICLES YOU MAY BE INTERESTED IN

Edge turbulence measurements in L-mode and I-mode at ASDEX Upgrade

R. Bielajew,[1,a),b)] G. D. Conway,[2] M. Griener,[2] T. Happel,[2] K. Höfler,[2,3] N. T. Howard,[1] A. E. Hubbard,[1]
W. McCarthy,[1] P. A. Molina Cabrera,[2] T. Nishizawa,[2] P. Rodriguez-Fernandez,[1] D. Silvagni,[2]
B. Vanovac,[2] D. Wendler,[2,3] C. Yoo,[1] A. E. White,[1] and ASDEX Upgrade Team[c)]

AFFILIATIONS

[1]MIT Plasma Science and Fusion Center, Cambridge, Massachusetts 02139, USA
[2]Max Planck Institute for Plasma Physics, 85748 Garching, Germany
[3]Physics Department E28, Technical University of Munich, 85748 Garching, Germany

Note: This paper is part of the Special Collection: Papers from the 63rd Annual Meeting of the APS Division of Plasma Physics.
Note: Paper JI1 1, Bull. Am. Phys. Soc. **66** (2021).
[a)]Invited speaker.
[b)]**Author to whom correspondence should be addressed:** bielajew@mit.edu
[c)]See author list of Meyer *et al.* Nucl. Fusion **59**, 112014 (2019). https://iopscience.iop.org/article/10.1088/1741-4326/ab18b8

ABSTRACT

The I-mode confinement regime is promising for future reactor operation due to high energy confinement without high particle confinement. However, the role of edge turbulence in creating I-mode's beneficial transport properties is still unknown. New measurements of edge turbulence ($\rho_{pol} = 0.9 - 1.0$) in L-modes and I-modes at low and high densities at ASDEX Upgrade are presented in this paper. A high radial resolution correlation electron cyclotron emission radiometer measures the broadband turbulence throughout the L-mode and I-mode edge and pedestal. The weakly coherent mode (WCM) is measured in both L-mode and I-mode near the last closed flux surface with T_e fluctuation levels of 2.3%–4.2%, with a frequency shift between the two phases related to a deeper E_r well in I-mode. An $n_e T_e$ phase diagnostic captures a change of the WCM $n_e T_e$ phase between L-mode and I-mode from $-171°$ to $-143°$. The thermal He beam diagnostic measures a WCM wavenumber range of -0.5 to $-1.0\,\text{cm}^{-1}$. A low-frequency edge oscillation (LFEO) appears in the I-mode phase of these discharges and displays coupling to the WCM, but the LFEO does not appear in the L-mode phase. Linear gyrokinetic simulations of the outer core and pedestal top turbulence indicate that while the dominant turbulent modes in the outer core are ion directed and electrostatic, the turbulence becomes increasingly electron directed and electromagnetic with increasing radius. Collisionality is not found to impact characteristics of the L-mode and I-mode edge turbulence with respect to the presence of the WCM; however, the quality of global confinement decreases with collisionality.

I. INTRODUCTION

The I-mode confinement regime is a promising operational regime for future fusion reactors because it features high energy confinement without the presence of edge-localized modes (ELMs). I-mode is characterized by the presence of an edge energy transport barrier (temperature pedestal) without an edge particle transport barrier (density pedestal).[1–3] The pedestal is, therefore, far from peeling–ballooning stability limits that lead to ELMs,[4–6] and the lack of a particle transport barrier prevents the accumulation of impurities. The I-mode regime is most commonly accessed in an unfavorable grad B drift configuration, which increases the power threshold for entering H-mode and thereby leaves a wider window for I-mode access. I-mode has been accessed in several machines (Alcator C-Mod, ASDEX Upgrade, DIII-D, and EAST)[1,3,7,8] and across a range of operational parameters such as density, q_{95}, magnetic field, collisionality, and heating scheme.

Properties of edge turbulence are believed to be important for overall confinement in high-performance operational regimes. For example, in ELMy H-mode, when turbulence is reduced within the edge transport barrier, high energy and particle confinement is

achieved. The nature of the edge and pedestal turbulence in I-mode plasmas is still under investigation. Open questions exist about the role of the turbulence in determining the transport of I-mode, in particular, the separation between the particle and energy transport channels. One feature commonly used to contrast L-mode with I-mode regimes is the change in pedestal fluctuations. I-mode is commonly accompanied by the weakly coherent mode (WCM), a localized pedestal fluctuation. The WCM occurs in a mid-frequency range (100–300 kHz on C-Mod and 50–150 kHz on ASDEX Upgrade).[1,3] The WCM has previously been suggested as an explanation for the beneficial transport properties of I-mode.[1,3] However, there are examples of I-modes in which the WCM is not measured,[9] and there are examples of the WCM in the L-mode phase preceding an I-mode phase.[10] Open questions exist about the role of the WCM in regulating the transport of the I-mode pedestal, and whether its presence is necessary for I-mode transport.

Identification of the WCM and its role in transport has been a focus of much previous I-mode work. The proposed explanations for the WCM vary widely. One drift wave-type instability that has been proposed to be responsible for the WCM and the impurity transport of I-mode is the heavy particle mode.[11] A gyrokinetic study of the I-mode edge at C-Mod found that the WCM could be an ion temperature gradient (ITG) or impurity mode, and this would be consistent with particle removal and heat transport properties of the I-mode edge.[12] Studies using the numerical fluid simulation code BOUT++ have found that the C-Mod I-mode pedestal is unstable to both the drift Alfvén wave instability and the resistive ballooning mode.[13] One other theorized regime of turbulence for I-mode is the reduction of electron heat transport with increasing conductivity, in which case the WCM is the residual broadband turbulence when large and small scales are stabilized and the resulting turbulence state is consistent with transport observations at ASDEX Upgrade.[14] In this model, as temperature increases, electrons become more adiabatic and fast parallel equilibration levels out electron temperature fluctuations. Sizeable electron temperature fluctuations associated with the WCM have been measured at both C-Mod and ASDEX Upgrade (AUG) although they are smaller in amplitude than density fluctuations.[3,15] Despite this dedicated WCM work, some literature has postulated that the WCM is not necessary to I-mode transport at Alcator C-Mod and that neoclassical transport alone can account for I-mode impurity transport.[16]

The frequency coupling between the WCM and modes at lower frequency has been observed on several machines. The coupling between the WCM and the geodesic acoustic mode (GAM) has been observed at C-Mod and AUG, with the GAM reported as the broadening mechanism for the WCM.[17,18] Low-frequency oscillations and an edge temperature ring oscillation have been identified in addition to the GAM during I-mode phases at EAST.[8,19,20] All three of these low-frequency modes are shown through bispectral analysis to couple to the WCM. The transfer of energy between background turbulence and zonal flows has been shown to be important in the L-mode to H-mode transition.[21] These nonlinear couplings may be important for the development of the WCM edge turbulence in the L-mode to I-mode transition as well.

In this paper, we investigate the role of collisionality and electron and ion temperature decoupling in determining the turbulence in the L-mode/I-mode edge, the role of the WCM in I-mode global confinement, and the characteristics of the WCM in L-mode and I-mode

through experimental work carried out at the ASDEX Upgrade tokamak. To measure electron temperature fluctuations across the outer core and pedestal, we use a correlation electron cyclotron emission (CECE) radiometer.[22] The high spatial resolution of this diagnostic captures the changes in turbulence in this region, from broadband turbulence inside the pedestal top to the highly localized WCM close to the separatrix. The thermal Helium beam diagnostic[23,24] complements CECE turbulence measurements by providing localized information about turbulence dispersion relations and phase velocity. Both these diagnostics also capture fluctuations associated with the newly observed low-frequency edge oscillation (LFEO)[25] in I-mode. In conjunction with fluctuation measurements, linear gyrokinetic simulations were performed with the CGYRO code.[26] These simulations allow a deeper probe into the nature of the edge turbulence, including identifying the radial location at which the turbulence changes from electrostatic to electromagnetic and dominantly ion to electron modes.

II. EXPERIMENTAL DESCRIPTION
A. Low-and high-density L-mode/I-mode discharges

In order to study the parameter space of collisionality, low- and high-density discharges with L-mode and I-mode phases were designed for a dedicated experiment. Plasma parameters for the two discharges are shown in Fig. 1. Both discharges have steady-state L-mode and I-mode phases, but they were designed with different densities and heating schemes. The "low n_e" L-mode/I-mode discharge was heated by electron cyclotron resonance heating (ECRH) in small power steps from L-mode to the I-mode threshold, and neutral beam injection (NBI) beam blips were present only for ion temperature measurements obtained with the charge exchange recombination spectroscopy (CXRS) system.[27] This discharge has a core line integrated density of $\sim 4.4 \times 10^{19}$ m^{-2}. The core density stays the same between the L-mode and I-mode phases, but the core electron temperature rises from ~ 3.0 keV in L-mode to ~ 4.0 keV in I-mode. The confinement enhancement factor H_{98} relative to the IPB98(y,2) scaling law[28] for the thermal confinement time rises from 0.70 in L-mode to 0.91 in I-mode.

The "high n_e" L-mode/I-mode discharge was designed with the I-mode phase first, followed by the L-mode phase. In contrast to the low n_e discharge, this plasma was heated by NBI feedback controlled on the β_{pol} value of the plasma with ECRH at a constant level of 1.4 MW. This discharge has a core line integrated density of $\bar{n}_e = 6.4 \times 10^{19}$ m^{-2}. The core electron temperature drops from ~ 2.5 keV in I-mode to ~ 1.8 keV in L-mode. The confinement of this discharge is comparatively worse than the low n_e case, with H_{98} reaching only 0.75 in I-mode and falling to 0.64 in L-mode.

The profile comparison of the two discharges is shown in Fig. 2. Integrated data analysis (IDA)[30] is used to determine n_e and T_e profile fits from standard profile diagnostics including Thomson scattering and 1D ECE. T_i profiles are made using CXRS data and Gaussian process regression (GPR) fits. The electron to ion temperature ratio T_e/T_i is determined from these fits, and the effective collisionality ν_{eff} is determined through the fitted profiles and Eq. (2) in Ref. 29:

$$\nu_{eff} = 0.002\,79 \times \left(15.94 - 0.5 \log \frac{n_e}{T_e^2}\right) \times \frac{n_e}{T_e^2} R\sqrt{m_A} Z_{eff}. \quad (1)$$

Both discharges display the characteristic n_e profiles that change minimally between L-mode and I-mode while the T_e and T_i profiles
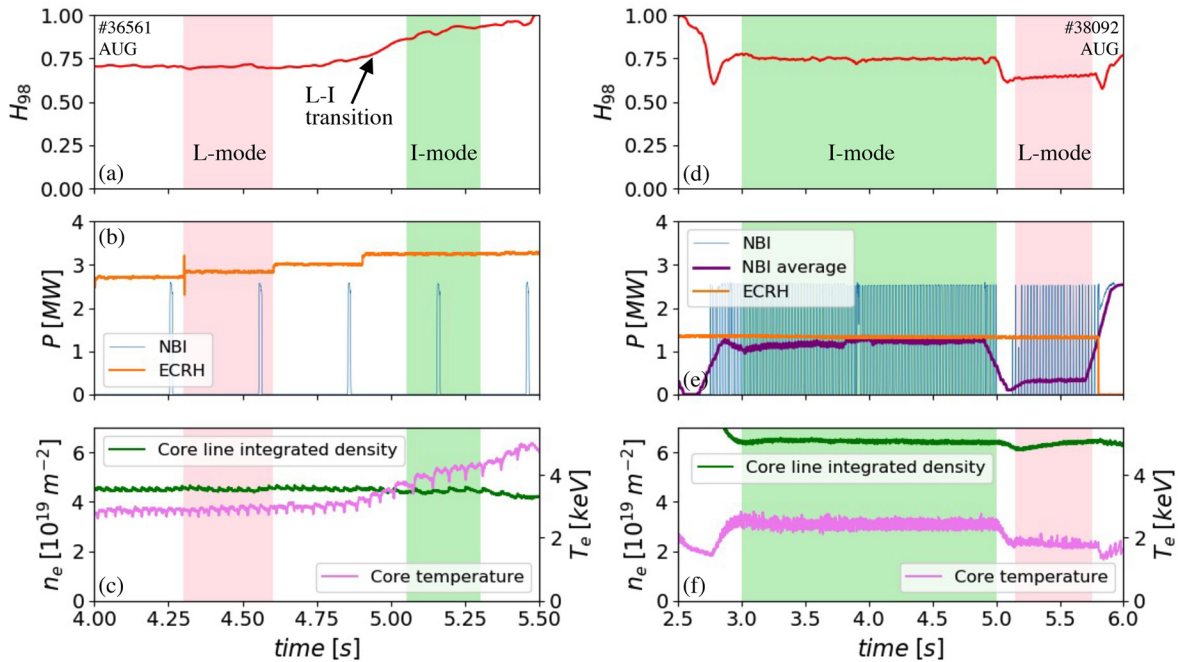
FIG. 1. Time histories of the low n_e (a)–(c) discharge 36 561 and the high n_e discharge (d)–(f) 38 092 with the phases of L-mode and I-mode used in the following turbulence analysis. (a) and (d) show the confinement improvement factor H_{98}. (b) and (e) show the heating schemes with ECRH steps and NBI beam blips in (b) and NBI in feedback with steady ECRH in (e). (c) shows the core line integrated electron density from DCN interferometry and (f) shows the on-axis temperature from core ECE. Both discharges display constant density in L-mode and I-mode with a higher temperature in I-mode than L-mode. The low n_e discharge has higher quality confinement than the high n_e discharge.

form a pedestal in I-mode. The low n_e discharge has a more marked development of a T_e pedestal in I-mode than the high n_e discharge, which displays a relatively weak T_e pedestal. The ion temperature in the L-mode phase of the high n_e discharge is taken from a previous discharge, which had matched parameters but more frequent CXRS ion measurements. The lower density and higher temperatures in the low n_e I-mode/L-mode case lead to lower collisionality than in the high n_e case. Collisionality is tied to the degree of electron and ion temperature coupling. The L-mode edges often have coupled T_e and T_i, while higher confinement regimes have decoupled edges due to higher temperatures and, therefore, lower collisionality. In the low n_e discharge, there is a change in coupling between the L-mode and I-mode edges as shown by the T_e/T_i ratios between L-mode and I-mode. The high n_e discharge has a higher degree of temperature coupling and little change in coupling between L-mode and I-mode.

The E_r profiles during the L-mode and I-mode phases of the low and high n_e discharges are shown in Fig. 3. The E_r profiles are measured using Doppler reflectometry.[31,32] In both the low and high n_e discharges, the E_r well deepens between L-mode and I-mode. The change in E_r slope leads to a change in sheared $E \times B$ flow in both cases. The E_r well is significantly deeper and wider in the low n_e I-mode than in the high n_e I-mode.

B. Experimental transport analysis

A simple experimental thermal transport analysis of the pedestal region was used following the method of Ref. 33 and shown in Table I.

The thermal diffusivity, χ_{eff}, is estimated with $\chi_{eff} = -P_{net}/(2An_e\nabla T_e)$ with P_{net} the power crossing the last closed flux surface (LCFS) and A the surface area of the LCFS. P_{net} is calculated as the heating input power minus the radiated power inside the LCFS as measured by bolometry. The experimental thermal diffusivities were estimated for the four different edges and pedestals of the low and high n_e L-modes and I-modes and shown in Table I, using the pedestal T_e gradient (taken from $\rho_{pol} = 0.96$ to 0.99) and mid-pedestal n_e value (taken at $\rho_{pol} = 0.975$). In both the low and high n_e discharges, the thermal diffusivity decreases with the increasing profile steepness from L-mode to I-mode. The fractional change in diffusivity between L-mode and I-mode phases is similar in both discharges. Lower thermal diffusivity values correspond with higher H_{98} and deeper E_r minimum values both when comparing L-mode to I-mode and when comparing low n_e cases with high n_e cases.

III. FLUCTUATION MEASUREMENTS

A. CECE T_e fluctuation measurements

The T_e fluctuations in these L-mode/I-mode discharges are primarily studied with the Correlation Electron Cyclotron Emission (CECE) diagnostic. The CECE diagnostic at AUG is a 24-channel heterodyne radiometer which receives 2nd harmonic X-mode radiation.[22,34] The IF filters have a bandwidth of 200 MHz and are spaced 250 MHz apart, which leads to a radial resolution of 2–4 mm between channels. The optics are shared with the 1D ECE at AUG, and they lead to a minimum beam width of diameter ∼1.4 cm, as determined by the $1/e^2$ power diameter. This sets a lower limit on the wavelength
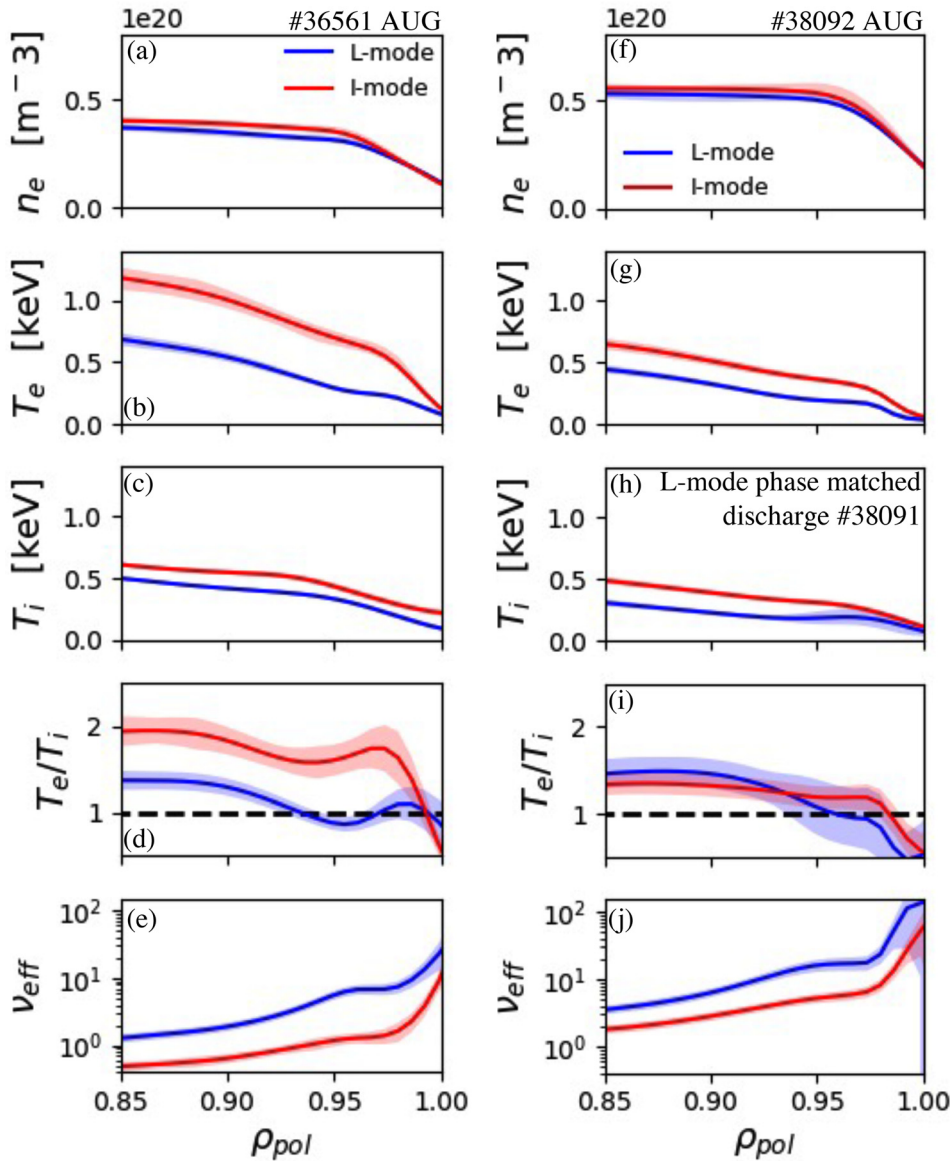
FIG. 2. Radial profiles of the low n_e (a)–(e) discharge 36 561 and the high n_e discharge (f) and (g) 38 092 from steady-state phases of L-mode and I-mode shown in Fig. 1. (a) and (f) electron density and (b) and (g) electron temperature from IDA. (c) and (h) ion temperature fitted with GPR. (d) and (i) electron to ion temperature ratios. (e) and (j) effective collisionality as defined in Ref. 29. The high n_e discharge displays lower T_e and T_i, stronger temperature coupling, and higher collisionality than the low n_e discharge.

to which the receiver is sensitive, and so, the CECE diagnostic is capable of measuring long-wavelength ($k_\theta \rho_s \lesssim 0.3$) turbulence.

Optical depth is a concern for ECE diagnostics in the cooler and lower-density plasma pedestal because when the plasma is optically thin, the collected emission intensity fluctuations may be due to a combination of density and temperature fluctuations. The potential impact of density fluctuations may be addressed through the procedure outlined in Ref. 35. For the fluctuations reported in this paper, temperature fluctuations are expected to be the dominant contribution to measured intensity fluctuations.

The T_e turbulence frequency spectra taken with the CECE diagnostic are shown in Fig. 4. The spectra show the absolute value of the complex coherency between neighboring CECE channels, with the location stated as the average location of the two correlated channels.

The fluctuation measurements span the outer core ($\rho_{pol} = 0.90$) through the LCFS, and the selection of these measurements shown in Fig. 4 displays the typical features of L-mode and I-mode turbulence in the outer core ($\rho_{pol} = 0.93$), inner pedestal top ($\rho_{pol} = 0.95$), and WCM location ($\rho_{pol} = 0.98$). The most prominent element in the spectra is the WCM, shown as the feature with the highest value of coherency in the pink spectra. In all cases studied, this mode is localized near $\rho_{pol} = 0.98$. In the low n_e discharge, the WCM is centered at 20 kHz in L-mode with a full-width half maximum (FWHM) of 40 kHz. In the low n_e I-mode, the WCM is centered at 90 kHz and has a FWHM of 120 kHz. In the high n_e L-mode, the WCM is centered at 40 kHz with a FWHM of 50 kHz and in the high n_e I-mode, and the WCM is centered at 60 kHz and has a FWHM of 90 kHz. The change in E_r between the I-mode and L-mode phases of the discharges is
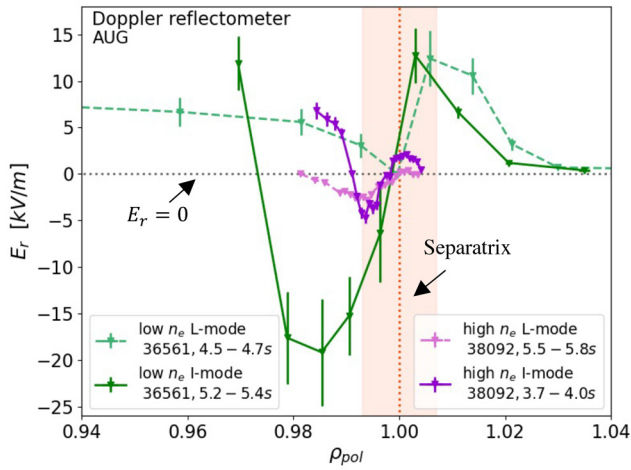
FIG. 3. Radial profiles of E_r for the low n_e discharge (36 561) and the high n_e discharge (38 092) as measured by Doppler reflectometers during I-mode and L-mode phases of these two discharges. Both discharges display a deepened E_r well in I-mode as compared to L-mode. The low n_e I-mode forms a much deeper well than the high n_e I-mode. The shaded region represents the maximum error on the separatrix position during these discharge phases.

TABLE I. Comparisons of thermal diffusivity, H_{98}, and the minimum value of E_r from Fig. 3. Experimental transport analysis of low- and high-density discharges to determine χ_{eff} uses T_e gradients and n_e values from the profiles in Fig. 2.

Shot	Phase	χ_{eff} (m^2/s)	H_{98}	E_r, min (kV/m)
Low n_e (36 561)	L	0.28	0.70	−0.04
	I	0.22	0.91	−19.18
High n_e (38 092)	L	0.36	0.66	−2.86
	I	0.27	0.75	−4.68

sufficient to increase the $E \times B$ flow and Doppler shift the spectra to higher frequencies, with a larger frequency shift occurring in the low n_e discharge with a larger change in E_r between L-mode and I-mode.

In addition to the WCM, broadband turbulence is seen on the CECE coherency spectra throughout the outer core and pedestal measurement locations ($\rho_{pol} = 0.90 - 0.97$). These broadband features, in some cases, shift frequency between L-mode and I-mode phases, such as the spectra at $\rho_{pol} = 0.93$ in the high n_e discharge but, generally, have a similar structure between L-mode and I-mode.

The normalized electron temperature fluctuation amplitude, dT_e/T_e, is derived from the integration of the coherency spectra,

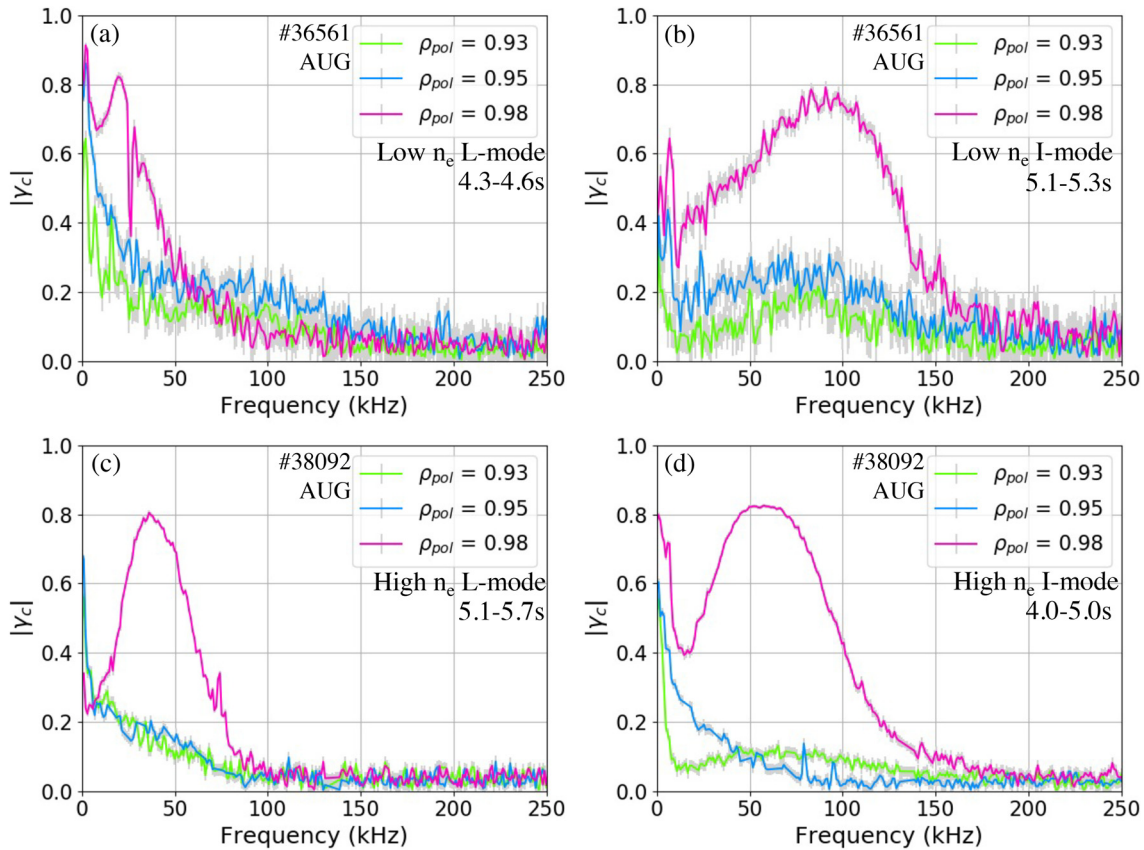**FIG. 4.** T_e fluctuation coherency spectra as measured by CECE in the low n_e discharge (36 561) (a) L-mode and (b) I-mode phases and the high n_e discharge (38 092) (c) L-mode and (d) I-mode phases. Spectra range from $\rho_{pol} = 0.93 - 0.98$. The WCM can be seen in all cases at $\rho_{pol} = 0.98$, and the broadband turbulence is seen in the outer core ($\rho_{pol} = 0.93$) and pedestal top ($\rho_{pol} = 0.95$) locations.

subtraction of the background coherency, and incorporation of IF filter bandwidth, as derived in Ref. 22. The profile dT_e/T_e over radius in the high and low n_e L-mode/I-mode phases is shown in Fig. 5. The WCM in L-mode and I-mode leads to a marked increase in fluctuation amplitude in the pedestal region. The fluctuation amplitude rises from close to 1% in the outer core to several times higher at the WCM location in all cases. In the low n_e case, the WCM fluctuation amplitude is 2.3% and 3.8% in L-mode and I-mode, respectively, and in the high n_e case is 2.8% and 4.2% in L-mode and I-mode, respectively. From these T_e fluctuation radial profiles, the WCM in both the low and high n_e cases, in both L-modes and I-modes, is localized at $\rho_{pol} \sim 0.97 - 0.99$. This corresponds in real space to a WCM width of around 1.8 cm. The regions of marginal optical depth ($\tau < 2$) are marked with a gray box. In all cases, the region of low optical depth occurs outside the region of peak WCM amplitude. The error bars typically associated with dT_e/T_e measurements are of a statistical nature and for these analyses of turbulence in the edge with high dT_e/T_e are, in many cases, smaller than the plotted points themselves.

The location of the E_r well can be compared from Fig. 3 with the WCM peak amplitude region from Fig. 5. In the low n_e I-mode, the E_r well extends the region from $\rho_{pol} = 0.97$ to the LCFS, and the WCM amplitude peaks just inside $\rho_{pol} = 0.98$. In the high n_e I-mode, the E_r well is farther toward the separatrix, centered around $\rho_{pol} = 0.99$, while the WCM once again peaks just inside $\rho_{pol} = 0.98$. These mappings indicate that the peak amplitude of the WCM occurs toward the

inside of the region of high $E \times B$ shear in I-mode but that the WCM persists throughout the E_r well region. These findings are consistent with previous WCM vs E_r localizations from EAST,[20] but they are inconsistent with findings from C-Mod, which place the WCM in the outer shear layer of the E_r well.[36] These localizations are subject to uncertainties in E_r locations due to density profile fits and CECE locations due to equilibrium reconstruction and mapping. The separatrix position has an uncertainty in position as large as 4.5 mm in these plasma phases, indicative of significant uncertainties in the mapping of edge CECE measurements and motivating a need for future studies.

The spectrogram of WCM fluctuations from the low n_e L-mode/I-mode discharge is shown in Fig. 6 using a single CECE channel at the location corresponding to the WCM peak amplitude ($\rho_{pol} \sim 0.98$). The WCM can be seen spinning up in frequency at the transition from L-mode to I-mode. At the onset of I-mode, a coherent low-frequency mode also appears (arrow on Fig. 6). This mode is identified as the LFEO.[25] The LFEO is also present in the high n_e I-mode phase. The LFEO amplitude peaks at the WCM location but has a larger radial extent than the WCM, appearing on CECE channels inside the pedestal top at $\rho_{pol} = 0.95$.

The LFEO appears only in the I-mode phase of these L-mode/I-mode discharges, with its onset occurring as the WCM ramps up to its I-mode frequency range. The presence does not appear to be ubiquitous in I-mode, as I-mode phases have been observed to occur without an observed LFEO.[25] In cases where the LFEO does appear in I-mode,
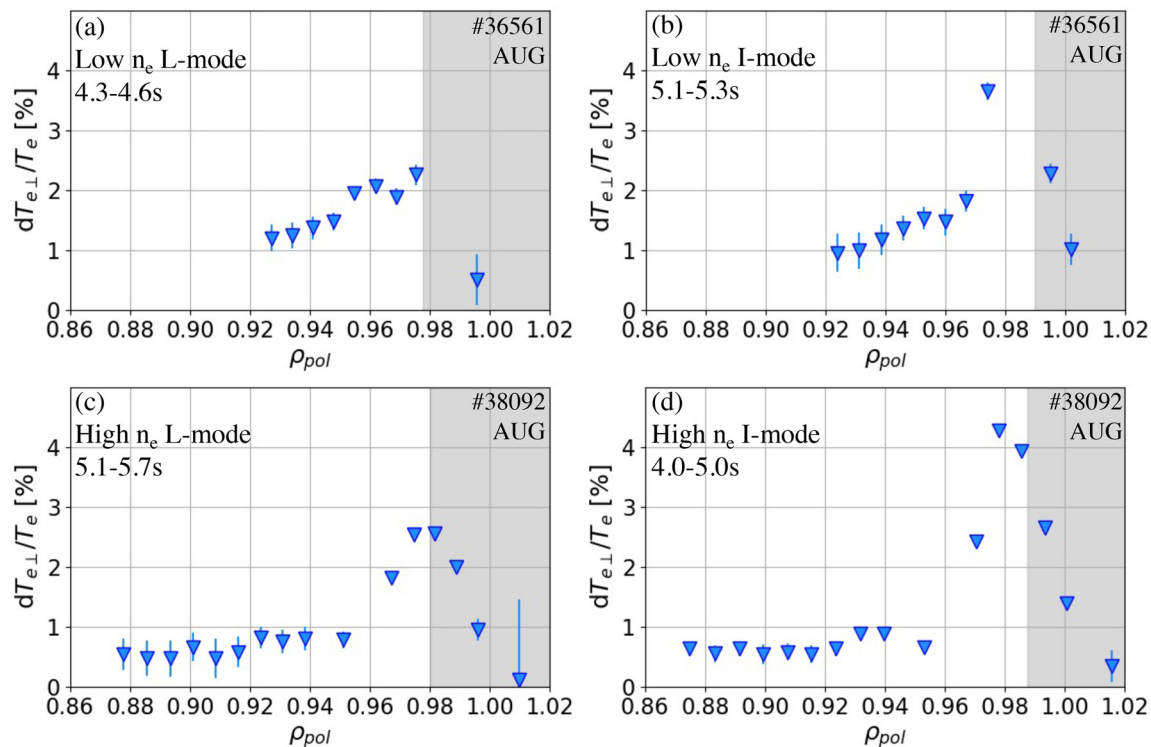
FIG. 5. Electron temperature fluctuation level over radius from low n_e discharge (36 561) (a) L-mode and (b) I-mode and the high n_e discharge (38 092) (c) L-mode and (d) I-mode. All phases use 10–250 kHz as the turbulence integration band and 250–270 kHz for background subtraction in the calculation of fluctuation amplitude. Regions of marginal optical depth $\tau < 2$ are shaded in gray. Fluctuation levels rise from $\sim$1% in the outer core to 2.3% $-$ 4.2% in the WCM range from $\rho_{pol} = 0.97 - 0.99$.
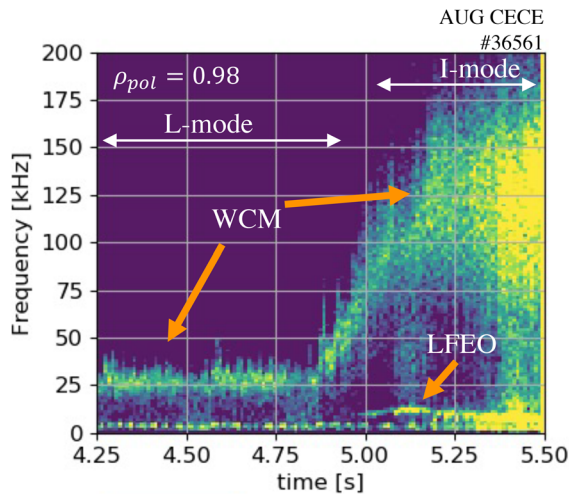
FIG. 6. Spectrogram from CECE channel 18 near the WCM peak amplitude of $\rho_{pol} = 0.98$ during the low n_e discharge (36 561). The WCM appears as the 25 kHz mode in L-mode which spins up to 80–160 kHz in I-mode, and the LFEO is the narrowband mode at 8 kHz which appears in the I-mode phase only.

it is coupled to the T_e turbulence associated with the WCM. Figure 7 shows the cross-bicoherence between neighboring CECE channels at the WCM location. The cross-bicoherence $\hat{b}$ of two fluctuation electron temperature signals $X(t)$ and $Y(t)$ is given by

$$\hat{b} = \sqrt{\frac{|\langle X(f_1)Y(f_2)X^*(f_1+f_2)\rangle|^2}{\langle |X(f_1)Y(f_2)|^2\rangle\langle |X^*(f_1+f_2)|^2\rangle}}, \qquad (2)$$

where $X(f)$ and $Y(f)$ are the Fourier transforms of $X(t)$ and $Y(t)$ and frequency coupling is investigated between f_1, f_2, and $f_1 + f_2$. This bicoherence analysis was applied to a medium n_e discharge (core line

integrated density of $\bar{n}_e = 5.3 \times 10^{19}$ m^{-2}) which was designed similar to the high n_e discharge for steady-state L-mode and I-mode phases and the WCM appeared in both phases. For the cross-bicoherence calculation, FFT bins of 4496 are used, with 1171 overlapping ensembles used for the L-mode period and 1855 used for the I-mode period. This analysis finds that in the L-mode phase of the discharge, despite the presence of the WCM, there is no three-wave coupling between different frequencies within the T_e fluctuation signals. In contrast, the I-mode phase displays coupling between the WCM frequency band (40–80 kHz) with the LFEO at ∼5 kHz. The coupling between the WCM and the LFEO is also seen in the auto-bicoherence of the thermal He beam channels during I-mode phases where these two fluctuations are present. Auto- and cross-bicoherence analysis does not give information about energy transfer between the coupled modes; however, frequency coupling is a prerequisite for the transfer of energy.

B. $n_e T_e$ phase measurements

The phase angle between electron density and temperature fluctuations ($\alpha_{n_e T_e}$) can be obtained with a reflectometer and CECE system that share a line of sight to the plasma. By choosing the appropriate frequencies for second harmonic EC emission and density cutoff, the reflectometer and radiometer can measure the same plasma volume.[34,37] The reflectometer does not share electronics other than the data acquisition board with the CECE system and does not suffer from thermal noise; therefore, a correlation between the reflectometer and radiometer signals will yield information about coherent turbulent quantities. Details of the $n_e T_e$ phase calculation and the associated uncertainty are found in Ref. 34.

Measurements of the $n_e T_e$ phase in L-mode and I-mode with a coupled CECE–reflectometer system find that the WCM has a finite negative $\alpha_{n_e T_e}$ in both L-mode and I-mode. For these measurements, an O-mode V-band reflectometer was used, and the reflectometer amplitude was used in correlating with the CECE signal. These measurements find that $\alpha_{n_e T_e}$ changes slightly between L-mode
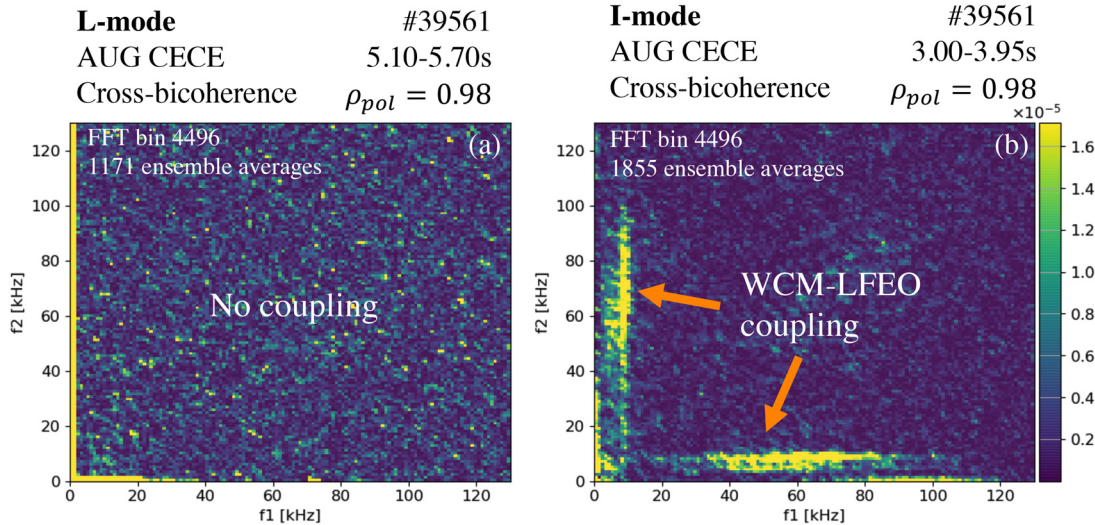

FIG. 7. Cross-bicoherence of neighboring CECE channels near the WCM peak location of $\rho_{pol} = 0.98$ during a medium density discharge (39 561). The L-mode phase (a) shows no coupling, while the I-mode phase (b) shows coupling between the WCM (40–60 kHz) and the LFEO (5 kHz).

and I-mode. The discharge in which these measurements were taken was the same medium density discharge shown in bicoherence analysis in Fig. 7. The coherency between CECE and reflectometer channels and the $n_e T_e$ phase during the L-mode and I-mode phases are shown in Fig. 8. The coherency spectra show that the fluctuations associated with the WCM are coherent between the radiometer and reflectometer. The $n_e T_e$ phase at the spectral peak of the WCM is $-171°$ in L-mode and shifts to $-143°$ in I-mode. The error associated with the $n_e T_e$ phase is of a statistical nature and is small in regions of coherency between the reflectometer and CECE, so this change in phase angle is statistically significant. It is possible that the measured values of $\alpha_{n_e T_e}$ could correspond to small or negative heat flux associated with the WCM and a positive particle flux, but the turbulent transport cannot be quantified without simultaneous measurements of the amplitude of fluctuations in T_e, n_e, plasma potential ϕ, magnetic field B, and $T_e - \phi$ and $n_e - \phi$ cross-phases. While $\alpha_{n_e T_e}$ does not enter directly into the turbulence-driven flux equations, comparisons of this measurement with theory and simulation will provide valuable new information about the physics of the WCM.

The $\alpha_{n_e T_e}$ measurement assists in quantifying the effects of density fluctuations in CECE measurements. To follow the analysis in Ref. 35, an n_e fluctuation level of 20% is assumed, corresponding with the upper limit of the WCM n_e fluctuations reported in Ref. 10. We then calculate the impact of n_e fluctuations on signal intensity if the T_e fluctuation level is 3%, in line with the typical CECE values for the AUG WCM. Reflective tungsten walls with a reflectivity value of $\chi = 0.85$ were assumed. The $n_e T_e$ phase angles measured in L-mode and I-mode were used in this calculation. The impact of n_e fluctuations

under these assumptions is shown in Fig. 9. The possibility of a greater than unity contribution of T_e fluctuations at low optical depth ($\tau_{2X} < 2$) is due to out of phase n_e fluctuations reducing the fluctuation signal intensity and leading to a smaller intensity fluctuation amplitude. In all WCM measurements presented in this paper, the peak WCM amplitude occurs in a region of high optical depth ($\tau_{2X} > 2$); therefore, CECE dT_e/T_e amplitude measurements are assumed to be robust and due primarily to T_e fluctuations with minimal impact from density fluctuations. There is a little change between L-mode and I-mode in terms of the impact of density fluctuations in regions of high optical depth. However, because the L-mode $n_e T_e$ phase is farther out of phase than the I-mode $n_e T_e$ phase, the interpretation of the WCM fluctuation amplitude in a marginal optical depth L-mode would be that the measured fluctuation intensity is likely slightly lower than the true dT_e/T_e amplitude.

C. Thermal helium beam measurements

The thermal helium (He) beam diagnostic is capable of measuring density and temperature fluctuations in the edge of AUG plasma.[23,24] Helium is injected into the plasma, and line ratio spectroscopy is performed to determine density and temperature. The diagnostic's 32 lines of sight enable correlation analysis.

The He beam diagnostic can capture information about the WCM poloidal structure and phase velocity, in addition to frequency spectra. Figure 10 shows the dispersion relation of edge fluctuations during the L-mode and I-mode phases of an additional medium-density L-mode/I-mode discharge (core line integrated density of
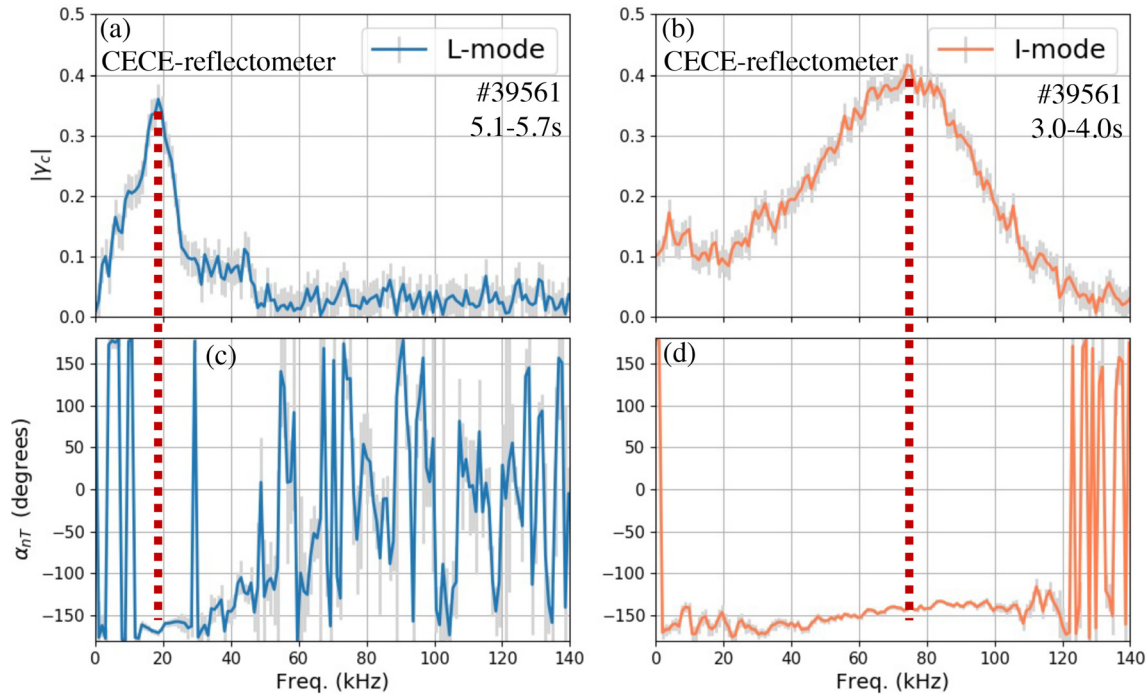

FIG. 8. Coherency between a CECE channel and V-band reflectometer at $\rho_{pol} = 0.97$ in the (a) L-mode and (b) I-mode phases of a middle density discharge (39 561) showing the WCM in both cases. (c) L-mode and (d) I-mode $n_e T_e$ phase over frequency. The $n_e T_e$ phase at the spectral peak of the WCM is $-171°$ in L-mode and shifts to $-143°$ in I-mode.
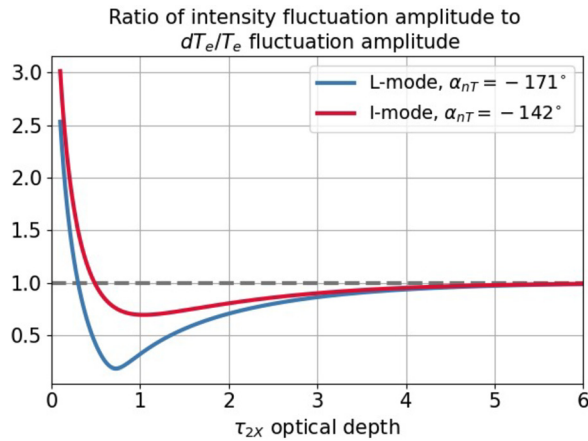
FIG. 9. Ratio of the CECE intensity fluctuation amplitude to the true dT_e/T_e fluctuation amplitude as a function of optical depth for two values of the n_eT_e cross-phase angle. For this toy calculation, the measured n_eT_e phases of the WCM in L-mode and I-mode were used, but estimates were used for fluctuation amplitudes ($dT_e/T_e = 3\%$ and $dn_e/n_e = 20\%$) and wall reflectivity ($\chi = 0.85$). At an optical depth of $\tau > 2$, the CECE intensity fluctuation amplitude corresponds well to the dT_e/T_e fluctuation amplitude.
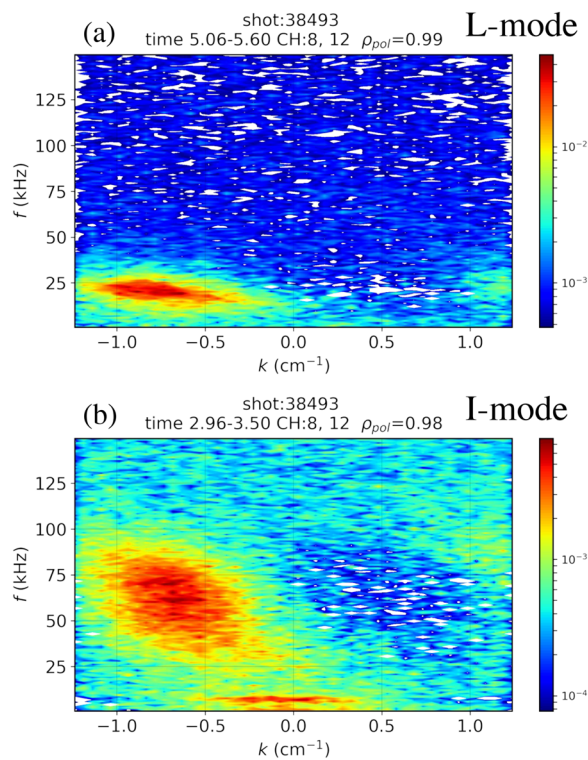

FIG. 10. Dispersion relation of fluctuations at $\rho_{pol} = 0.98$ and 0.99 from poloidally separated channels of the thermal Helium beam. The WCM is seen in the L-mode phase (a) at 25 KHz and the I-mode phase (b) at 45–75 kHz. The wavenumber extent of the WCM does not change between L-mode and I-mode, and the frequency change is consistent with a Doppler shift between the two regimes. The LFEO also appears in the I-mode phase at 4 kHz.

$\bar{n}_e = 5.1 \times 10^{19}\,\mathrm{m}^{-2}$) with steady-state L-mode and I-mode phases. This dispersion relation was calculated from poloidally separated channels using the spectral analysis method from Ref. 38. The WCM is the feature with wavenumbers in the range of -0.5 to $-1.5\,\mathrm{cm}^{-1}$, and the wavenumber extent stays the same between L-mode and I-mode. These wavenumbers are similar to the WCM wavenumber extent reported from a similar analysis on C-Mod and AUG.[17,39] The WCM is centered around a frequency of $\sim$20 kHz in L-mode and broadening to the range of 30–90 kHz in I-mode with a peak amplitude at $\sim$60 kHz. This frequency shift of the WCM between L-mode and I-mode is again consistent with a Doppler shift due to increased $E \times B$ velocity, with a larger frequency shift occurring at a larger wavenumber absolute value. The structure that appears near 4 kHz centered around $k = 0\,\mathrm{cm}^{-1}$ is the LFEO and appears in the I-mode phase only. This spectral analysis was applied to channels, which were not neighboring but rather poloidally separated by $\sim$2.5 cm. This indicates a high amount of poloidal coherency of the WCM and the LFEO.

The He beam diagnostic can also determine the WCM phase velocity by using the phase angle between coherent fluctuations in poloidally separated channels and the spacing between the channels. During the L-mode phase of this mid n_e discharge, the WCM fluctuation peak at $\sim$20 kHz propagates with a velocity of ~ -1.5 km/s. The negative sign indicates the electron diamagnetic direction. During the I-mode phase, the WCM peak at $\sim$60 kHz propagates at ~ -6 km/s. This change of -4.5 km/s in velocity is consistent with a change in the $E \times B$ flow resulting from the decrease in E_r from L-mode to I-mode. These WCM phase velocity measurements include the contribution from the plasma flow, so plasma poloidal velocity measurements are needed in order to determine the magnitude and direction of the WCM in the plasma frame.

IV. GYROKINETIC ANALYSIS

The low and high n_e L-mode and I-mode discharges studied experimentally in this paper were investigated using the gyrokinetic code CGYRO.[26] A summary of the input parameters for the simulations performed is given in the Appendix. The modeling focused on the same region of plasma as the CECE measurements covering the plasma edge from the outer core to the pedestal top region; however, modeling was not performed in the steep pedestal region. The low and high n_e L-mode and I-mode phases were studied by linear stability analysis in order to compare qualitatively the dominant mode behavior across this parameter space. This gyrokinetic work is intended to provide a deeper understanding of the turbulence physics but was not a validation exercise for direct comparison with experimental measurements.

Dominant mode growth rates and real frequencies over $k_\theta \rho_s$, where k_θ is the wavenumber in the poloidal direction and ρ_s is the ion sound gyroradius, are shown in Fig. 11. This figure shows the low-wavenumber portion of the spectrum at four locations representing the outer core ($\rho_{pol} = 0.90$ and 0.93) and pedestal top location ($\rho_{pol} = 0.95$ and 0.96). Of these locations, the outer core is the only location that features ion-directed modes in the ITG-scale portion of the normalized wavenumber $k_\theta \rho_s$ spectrum, and this is common to all four plasma phases studied. At the pedestal top and throughout the pedestal, the dominant mode becomes electron directed, which is similar to the findings in Ref. 40. Scans of the ion temperature gradient indicate that the pedestal top modes in all cases are robustly electron
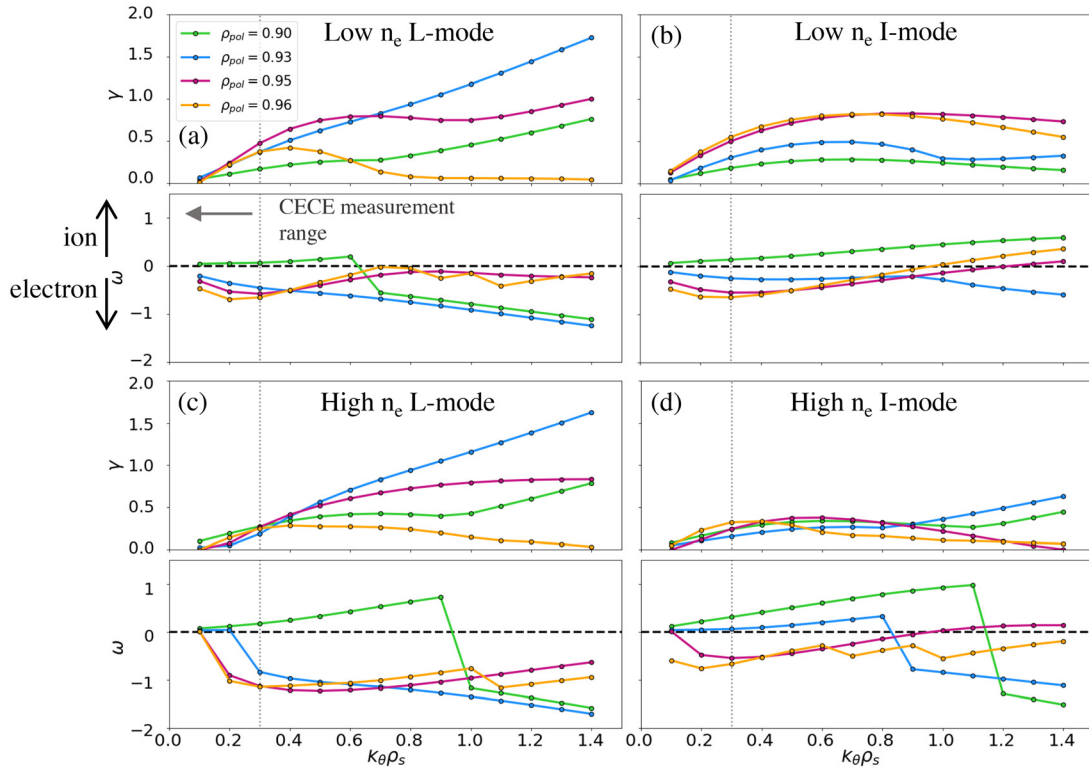
FIG. 11. Linear stability results of the low n_e discharge (36 561) during (a) L-mode and (b) I-mode and the high n_e discharge (38 092) during (c) L-mode and (d) I-mode using input profiles from Fig. 2. Growth rates γ and real frequencies ω shown at $\rho_{pol} = 0.90$, 0.93, 0.95, and 0.96. Negative ω indicates electron diamagnetic direction, and positive ω indicates ion diamagnetic direction. In the CECE measurement range, modes become more electron directed with radius, with ion-directed modes only occurring at the outer core locations.

directed because even at ion temperature gradients twice the experimental value, the modes remained electron directed. The normalized inverse gradient scale length is larger for the electron temperature than both density and ion temperature in all cases and may play a role in the prevalence of electron modes, but there are no obvious trends with radius. In all cases, the $E \times B$ shearing rate is less than 6×10^{-2} in units normalized by a/c_s as with γ, so it is exceeded by dominant mode growth rates at all radii for almost all $k_\theta \rho_s$.

At the ion scale, electromagnetic effects become more important with radius in all plasmas studied, as shown in Fig. 12. This is quantified with the change between electrostatic and electromagnetic runs in growth rate and real frequency of ion-scale modes at $k_\theta \rho_s = 0.3$. The outer core locations display almost no change in growth rate γ and real frequency ω between electrostatic and electromagnetic runs, meaning these core plasma locations are primarily electrostatic, while electromagnetic effects become larger throughout the pedestal. The electromagnetic nature of the I-mode plasmas was stronger than that of the L-mode plasmas, possibly as a result of a higher β.

Electron-scale linear stability analysis was also performed in the outer core for the low and high n_e L-mode and I-mode phases. The dominant mode growth rates are found to decrease from the L-mode to the I-mode phase in both cases, in contrast to Ref. 40. A larger fractional decrease in growth rate occurs in the low n_e scenario than the high n_e scenario, as shown in Fig. 13 which displays growth rate γ over electron-scale wavenumbers at the radial location $\rho_{pol} = 0.93$. This trend also

holds for other simulated radial locations and can be observed in the portion of the ion-scale spectra (Fig. 11) above $k_\theta \rho_s = 0.3$. The electron temperature inverse gradient scale lengths are larger in L-mode than in I-mode in the outer core where the simulations are performed, which
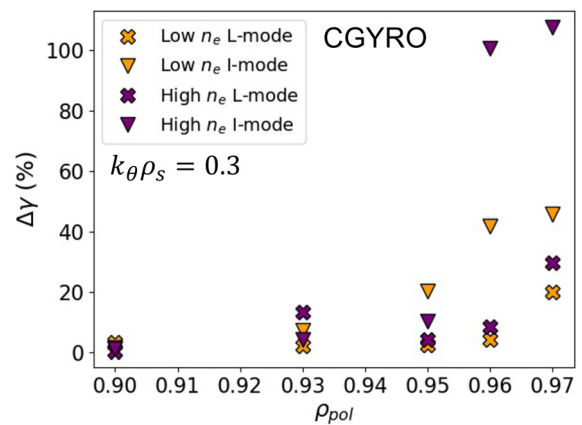

FIG. 12. Percentage change in dominant mode growth rate at $k_\theta \rho_s = 0.3$ between electrostatic and electromagnetic linear CGYRO simulations. The change in growth rate becomes larger with increasing radius, indicating that electromagnetic effects become more important.
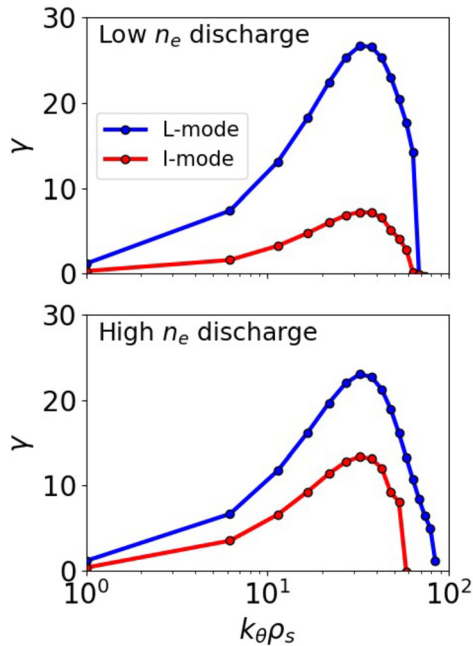
FIG. 13. Linear stability analysis results of the dominant electron scale mode of the high and low n_e discharges at the radial position $\rho_{pol} = 0.93$. The growth rate of the dominant mode decreases in I-mode as compared to L-mode, with a more marked decrease occurring in the low n_e case.

may fully explain the decrease in electron-scale growth rates in that radial region. The change in the gradient scale lengths occurs because the electron temperature is higher in I-mode than L-mode in this region, even though the gradients do not change significantly. We do not expect that this would be the case further out radially in the steep gradient region. Such near-edge simulations are left for future work.

V. DISCUSSION

In this work, plasmas with WCMs in L-mode and I-mode were specially designed to study the effects of collisionality on edge turbulence and transport and global confinement. Several observations from the discharges studied in this paper indicate that the WCM is the same instability in L-mode and I-mode: The L-mode and I-mode versions of the WCM are observed at the same radial location on the same CECE channels, the change in mode frequency between L-mode and I-mode can be explained by increased $E \times B$ flow, and the WCM exists at the same poloidal wavenumbers in L-mode and I-mode. The presence of the WCM in both regimes is not inconsistent with the paradigm of equivalent particle transport between the two regimes since the WCM could be driving particle transport in both cases.

The LFEO[25] that is present in I-mode and L-mode is the subject of current investigation.[41] Here, we note that the presence of the LFEO in I-mode and not L-mode, despite the presence of the WCM in L-mode, indicates that this low-frequency oscillation may play an important role in the development or sustainment of I-mode. WCM–LFEO coupling may be important and must be further studied to understand its implications on transport. Neither the LFEO nor the GAM is always present in I-modes, but of these two low-frequency

fluctuations, the LFEO appears to be unique to I-mode. Because the LFEO is distinct from the standard GAM, one possible identification for this fluctuation is a finite frequency flow oscillation (ZFO). Properties of the LFEO which are consistent with a ZFO include its presence in a region of significant $E \times B$ flow and pressure gradient, its coupling to WCM turbulence, and its frequency below that expected for a GAM.[42] Studies of the nonlinear transfer of energy between the LFEO and the WCM as in Ref. 17 and further identification of the properties of the LFEO will be important in understanding the details of the interaction between the WCM and the LFEO.

The plasmas studied in this paper had a range of collisionality and confinement (given by H_{98}) values, but the edge and pedestal turbulence had similarities in fluctuation level over radius and frequency spectra appearance in all the cases. A small database of plasmas in which edge turbulence was investigated with CECE is shown in the parameter space of collisionality and H_{98} in Fig. 14. These plasmas all displayed L-mode and I-mode phases with a WCM. The confinement is negatively correlated with collisionality in these plasmas, which is also observed in other devices and confinement regimes.[43,44] The trend is the same when using instead the H_{89} confinement enhancement factor calculated with L-mode scaling.[45] The presence of the WCM is not correlated with either collisionality or confinement. The low-k turbulence studied with CGYRO also does not appear to be significantly affected by collisionality in terms of dominant mode nature although nonlinear simulations would be needed to understand if there is an effect of collisionality on the saturated turbulence. The impact of collisionality on the high-k modes in these plasmas is still unknown but could be an explanation for a change in confinement quality that is not visible in turbulence at the ion-scale. Collisionality and the T_e/T_i ratio are important for the prevalence of electron temperature gradient (ETG) vs trapped electron mode (TEM) turbulence in the high-k regime[46]

The WCM dT_e/T_e fluctuation level is generally higher in the I-mode phase than in that plasma's corresponding L-mode phase, but within the L-mode and I-mode phases alone, there is no correlation between collisionality and WCM dT_e/T_e amplitude or confinement and WCM dT_e/T_e amplitude. Considering the values in Table I, WCM presence or fluctuation level also cannot be correlated with thermal diffusivity or E_r well depth. This suggests that the WCM does not play a role in heat transport and energy confinement in these plasmas. The existence and consistent properties of the WCM over this entire parameter space motivate further study to determine the parameters to which this fluctuation is sensitive.

The T_e turbulence in the outer core and pedestal top has similar fluctuation levels in L-mode and I-mode and displays similar broadband features of drift wave turbulence in frequency spectra in L-mode and I-mode (Figs. 4 and 5). Linear gyrokinetic linear simulations also suggest qualitatively similar behavior at ion scales between L-mode and I-mode dominant modes, in terms of modes becoming more electron directed and more electromagnetic with radius. We note that these ion-scale trends are observed here in linear simulations, and their effect on heat flux, if any, would require nonlinear simulations. The dominant mode growth rates at $k_\theta \rho_s < 0.3$, the range where CECE and He beam measure fluctuations, do not change significantly between L-mode and I-mode. As discussed, the pedestal WCM is also qualitatively similar between L-mode and I-mode.

The similarity in this ion-scale T_e turbulence across the transition in confinement and as the E_r well and T_e pedestal form suggests that
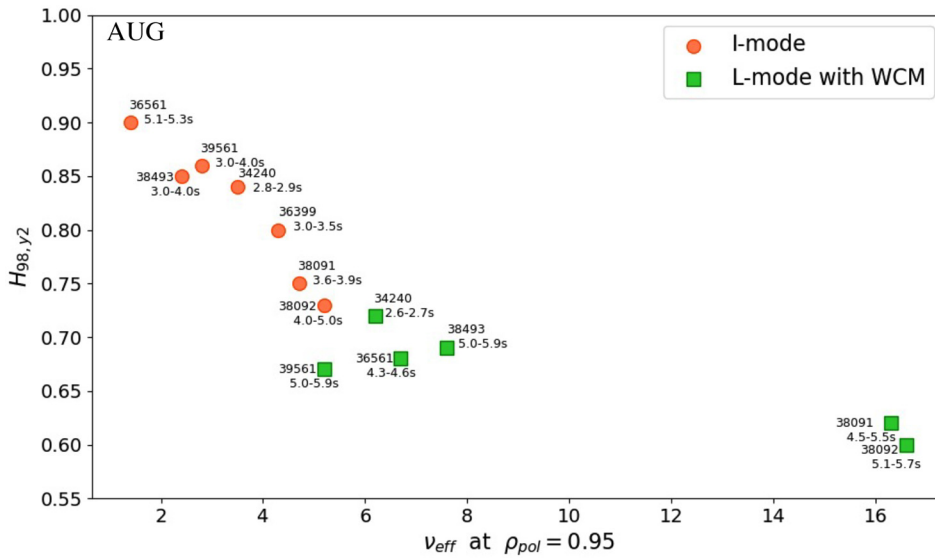
FIG. 14. Confinement improvement factor $H_{98,y2}$ plotted against effective collisionality ν_{eff} evaluated at $\rho_{pol} = 0.95$. All discharges plotted here have CECE measurements of the WCM in both L-mode and I-mode. Negative correlation is observed between confinement and effective collisionality for these discharges.

the explanation for improved energy confinement may lie in other channels besides the ion-scale T_e turbulence. The linear gyrokinetic analysis shows that the dominant mode growth rates at higher $k_\theta \rho_s$, most notably in the ETG portion of the spectrum, do decrease between L-mode and I-mode. This suggests that a possible explanation for improved energy confinement of I-mode compared to L-mode could be the suppression of small-scale turbulence. Further investigation of the reduction in electron scale turbulence will require an extension to pedestal simulations and nonlinear gyrokinetic investigation. The widely previously reported explanation for the improvement in energy confinement has been the reduction in fluctuations in the density channel at frequencies lower than the WCM, while this work has focused on T_e fluctuations, which are more rarely reported in edge turbulence studies. The density to temperature fluctuation ratio of broadband fluctuations and the WCM across the L-mode to I-mode transition may be important in understanding changes in transport and is left for future work.

The measurements presented in this work illustrate the gradual nature of the transition in turbulence between L-mode and I-mode, in contrast to the marked transition between L-mode and H-mode. Edge gradients and normalized gradients (e.g., ∇T_e and $\nabla T_e / T_e$) can, in some cases, be comparable in I-mode and L-mode phases. The slight increase in WCM T_e fluctuation amplitude between L-mode and I-mode coupled with the fact that the WCM amplitude peaks toward the inside of the E_r well region gives a picture that is consistent with typical turbulence drive and damping mechanisms across a smoothly transitioning parameter space. The apparent decrease of the WCM dT_e / T_e fluctuation amplitude close to the separatrix may be related to the strong $E \times B$ shear in this region; however, this region of the plasma is not optically thick, so CECE measurements may have contributions from electron density fluctuations as well as electron temperature fluctuations. Gyrokinetic modeling is also challenging to perform at this radial location. This near-separatrix region may play a critical role in the confinement improvement between L-mode and I-mode. The dynamics of the transport barrier formation and the LFEO at the onset of I-mode must still be understood.

The comparisons between the different L-mode/I-mode plasmas studied allow for observations of turbulence core-edge coupling. The low n_e discharge presented, which had high quality confinement in I-mode with $H_{98} = 0.91$, featured the formation of a deep E_r well in I-mode as well as a slight reduction of outer core turbulence. The dT_e / T_e fluctuation amplitude decreased on average by 15% for CECE measurements inside of $\rho_{pol} = 0.95$. This decrease in core fluctuation amplitude is of a similar magnitude to observations of core turbulence in C-Mod I-modes.[47] In comparison, the high n_e discharge had poorer quality confinement with $H_{98} = 0.75$ and featured a shallower I-mode E_r well and an increase in dT_e / T_e of 11% on average for radii inside of $\rho_{pol} = 0.95$ between L-mode and I-mode. These results highlight the possible importance of core-edge coupling in the transition to high confinement regimes and the role of both core and edge turbulence in determining global confinement properties.

VI. SUMMARY AND CONCLUSIONS

Edge turbulence in L-mode and I-mode was studied with the CECE, $n_e T_e$ cross phase, and thermal He beam diagnostics at ASDEX Upgrade. In order to study the parameter space of collisionality, discharges were designed at a variety of densities. Edge turbulence, in particular, the WCM, was found to be qualitatively unchanged across this parameter space.

No major changes in turbulence were observed experimentally between L-mode and I-mode with respect to the appearance of the WCM in T_e fluctuation signals or the wavenumbers of the WCM. Slight changes occurred in the electron temperature fluctuation amplitude and the $n_e T_e$ phase between L-mode and I-mode. Linear gyrokinetic studies found turbulence deeper into the core was also similar between L-mode and I-mode in the ion scale, but dominant mode linear growth rates of electron scale modes are suppressed in I-mode. One marked difference between L-mode and I-mode was the coupling between the WCM and the LFEO, which occurred only in I-mode. This low-frequency mode was present in these discharges but is not present in all I-mode discharges at AUG, so, this is a direction for future work. Globally, we found that while E_r well depth was correlated

with confinement, and collisionality was correlated with confinement, the appearance of the WCM was not correlated with E_r well depth or collisionality. The WCM is, therefore, likely to be an instability that is insensitive to collisionality.

Further work is needed to understand density to temperature fluctuation ratios across the L-mode to I-mode transition, determine the conditions that lead to the WCM's existence in L-mode, and understand how core-edge coupling is important in the confinement transition. Additional investigation of the role of the LFEO is needed in order to determine whether this low-frequency mode or its coupling to the WCM has implications for I-mode transport.

ACKNOWLEDGMENTS

AUTHOR DECLARATIONS
Conflict of Interest

The authors have no conflicts to disclose.

DATA AVAILABILITY

The data that support the findings of this study are available from the corresponding author upon reasonable request.

APPENDIX: SUMMARY OF SIMULATION INPUTS

Input parameters for the linear CGYRO simulations presented in this work are presented in Tables II–V.

TABLE II. Gyrokinetic input parameters at $\rho_{pol} = 0.90$.

	Low n_e		High n_e	
	L-mode	I-mode	L-mode	I-mode
n_e (10^{19} m^{-3})	3.52	3.96	5.22	5.69
T_e (keV)	0.54	1.04	0.36	0.54
T_i/T_e	0.79	0.53	0.63	0.74
a/L_n	1.18	0.58	0.37	−0.16
a/L_{T_e}	5.23	2.68	6.01	4.08
a/L_{T_i}	2.89	2.77	5.04	3.69
Z_{eff}	1.11	1.40	1.07	1.07
$\nu_{ee}(a/c_s)$	0.49	0.15	1.66	0.79
q	−2.45	−2.50	−2.53	−2.65

TABLE II. (*Continued.*)

	Low n_e		High n_e	
	L-mode	I-mode	L-mode	I-mode
$\hat{s}$	2.39	2.50	2.30	2.11
$\gamma_{E\times B}(a/c_s)$	0.02	0.02	0.01	0.05
$\gamma_p(a/c_s)$	−0.19	−0.18	−0.12	−0.55
$\beta_e \times 10^{-3}$	0.44	0.94	0.43	0.64

TABLE III. Gyrokinetic input parameters at $\rho_{pol} = 0.93$.

	Low n_e		High n_e	
	L-mode	I-mode	L-mode	I-mode
n_e (10^{19} m^{-3})	3.32	3.78	5.25	5.63
T_e (keV)	0.40	0.87	0.26	0.42
T_i/T_e	0.93	0.55	0.72	0.77
a/L_n	1.74	2.00	1.37	1.21
a/L_{T_e}	8.61	4.49	8.27	4.22
a/L_{T_i}	3.61	3.17	3.23	2.98
Z_{eff}	1.11	1.40	1.07	1.07
$\nu_{ee}(a/c_s)$	0.83	0.21	2.99	1.19
q	−2.78	−2.86	−2.85	−3.01
$\hat{s}$	2.81	2.91	2.79	2.54
$\gamma_{E\times B}(a/c_s)$	0.02	0.02	0.01	0.06
$\gamma_p(a/c_s)$	−0.22	−0.18	−0.14	−0.66
$\beta_e \times 10^{-3}$	0.27	0.65	0.27	0.45

TABLE IV. Gyrokinetic input parameters at $\rho_{pol} = 0.95$.

	Low n_e		High n_e	
	L-mode	I-mode	L-mode	I-mode
n_e (10^{19} m^{-3})	3.05	3.39	4.84	5.28
T_e (keV)	0.30	0.74	0.21	0.39
T_i/T_e	1.09	0.58	0.89	0.80
a/L_n	3.93	5.12	3.91	3.85
a/L_{T_e}	8.24	6.00	4.96	4.01
a/L_{T_i}	4.73	3.59	−1.96	2.80
Z_{eff}	1.11	1.40	1.07	1.07
$\nu_{ee}(a/c_s)$	1.35	0.25	4.32	1.38
q	−3.11	−3.20	−3.21	−3.27
$\hat{s}$	3.41	3.31	3.40	2.89
$\gamma_{E\times B}(a/c_s)$	0.02	0.02	0.01	0.06
$\gamma_p(a/c_s)$	−0.24	−0.19	−0.15	−0.69
$\beta_e \times 10^{-3}$	0.16	0.44	0.17	0.34

TABLE V. Gyrokinetic input parameters at $\rho_{pol} = 0.96$.

	Low n_e		High n_e	
	L-mode	I-mode	L-mode	I-mode
n_e (10^{19} m^{-3})	2.19	3.07	4.50	4.69
T_e (keV)	0.26	0.66	0.19	0.35
T_i/T_e	1.13	0.61	0.98	0.82
a/L_n	6.04	7.54	5.82	7.13
a/L_{T_e}	6.74	8.38	4.49	7.29
a/L_{T_i}	5.58	4.01	-0.84	6.17
Z_{eff}	1.11	1.40	1.07	1.07
$\nu_{ee}(a/c_s)$	1.58	0.29	4.59	1.53
q	-3.31	-3.39	-3.40	-3.51
$\hat{s}$	3.81	3.58	3.73	3.27
$\gamma_{E\times B}(a/c_s)$	0.02	0.02	0.01	0.06
$\gamma_p(a/c_s)$	-0.26	-0.20	-0.15	-0.72
$\beta_e \times 10^{-3}$	0.12	0.33	0.14	0.25

REFERENCES

[1]D. Whyte, A. Hubbard, J. Hughes, B. Lipschultz, J. Rice, E. Marmar, M. Greenwald, I. Cziegler, A. Dominguez, T. Golfinopoulos, N. Howard, L. Lin, R. McDermott, M. Porkolab, M. Reinke, J. Terry, N. Tsujii, S. Wolfe, S. Wukitch, and Y. Lin, "I-mode: An H-mode energy confinement regime with L-mode particle transport in Alcator C-Mod," Nucl. Fusion **50**, 105005 (2010).

[2]A. E. Hubbard, D. G. Whyte, R. M. Churchill, I. Cziegler, A. Dominguez, T. Golfinopoulos, J. W. Hughes, J. E. Rice, I. Bespamyatnov, M. J. Greenwald, N. Howard, B. Lipschultz, E. S. Marmar, M. L. Reinke, W. L. Rowan, and J. L. Terry, "Edge energy transport barrier and turbulence in the I-mode regime on Alcator C-Mod," Phys. Plasmas **18**, 056115 (2011).

[3]T. Happel, P. Manz, F. Ryter, P. Hennequin, A. Hetzenecker, G. Conway, L. Guimarais, C. Honoré, U. Stroth, and E. Viezzer, "Turbulence intermittency linked to the weakly coherent mode in ASDEX Upgrade I-mode plasmas," Nucl. Fusion **56**, 064004 (2016).

[4]J. R. Walk, J. W. Hughes, A. E. Hubbard, J. L. Terry, D. G. Whyte, A. E. White, S. G. Baek, M. L. Reinke, C. Theiler, R. M. Churchill, J. E. Rice, P. B. Snyder, T. Osborne, A. Dominguez, and I. Cziegler, "Edge-localized mode avoidance and pedestal structure in I-mode plasmas," Phys. Plasmas **21**, 056103 (2014).

[5]T. Happel, P. Manz, F. Ryter, M. Bernert, M. Dunne, P. Hennequin, A. Hetzenecker, U. Stroth, G. D. Conway, L. Guimarais, C. Honoré, and E. Viezzer, "The I-mode confinement regime at ASDEX Upgrade: Global properties and characterization of strongly intermittent density fluctuations," Plasma Phys. Controlled Fusion **59**, 014004 (2017).

[6]D. Silvagni, T. Eich, T. Happel, G. Harrer, M. Griener, M. Dunne, M. Cavedon, M. Faitsch, L. Gil, D. Nille, B. Tal, R. Fischer, U. Stroth, D. Brida, P. David, P. Manz, and E. Viezzer, "I-mode pedestal relaxation events at ASDEX Upgrade," Nucl. Fusion **60**, 126028 (2020).

[7]A. Marinoni, J. Rost, M. Porkolab, A. Hubbard, T. Osborne, A. White, D. Whyte, T. Rhodes, E. Davis, D. Ernst, and K. Burrell, "Characterization of density fluctuations during the search for an I-mode regime on the DIII-D tokamak," Nucl. Fusion **55**, 093019 (2015).

[8]Y. Liu, Z. Liu, A. Liu, C. Zhou, X. Feng, Y. Yang, T. Zhang, T. Xia, H. Liu, M. Wu, X. Zou, D. Kong, H. Li, J. Xie, T. Lan, W. Mao, S. Zhang, W. Ding, G. Zhuang, and W. Liu, "Power threshold and confinement of the I-mode in the EAST tokamak," Nucl. Fusion **60**, 082003 (2020).

[9]J. Walk, A. Hubbard, D. Whyte, and A. White, in 57th Annual Meeting of the APS Division of Plasma Physics, 2015.

[10]T. Happel, M. Griener, D. Silvagni, S. J. Freethy, P. Hennequin, F. Janky, P. Manz, D. Prisiazhniuk, F. Ryter, M. Bernert, D. Brida, T. Eich, M. Faitsch, L. Gil, L. Guimarais, A. Merle, D. Nille, J. Pinzón, B. Sieglin, U. Stroth, and E.

Viezzer, "Stationarity of I-mode operation and I-mode divertor heat fluxes on the ASDEX Upgrade tokamak," Nucl. Mater. Energy **18**, 159–165 (2019).

[11]B. Coppi, H. P. Furth, M. N. Rosenbluth, and R. Z. Sagdeev, "Drift instability due to impurity ions," Phys. Rev. Lett. **17**, 377–379 (1966).

[12]X. Liu, M. Kotschenreuther, D. R. Hatch, S. M. Mahajan, J. W. Hughes, and A. E. Hubbard, "Gyrokinetics investigations of an I-mode pedestal on Alcator C-Mod," arXiv:2005.08924 (2020).

[13]Z. X. Liu, X. Q. Xu, X. Gao, A. E. Hubbard, J. W. Hughes, J. R. Walk, C. Theiler, T. Y. Xia, S. G. Baek, T. Golfinopoulos, D. Whyte, T. Zhang, and J. G. Li, "The physics mechanisms of the weakly coherent mode in the Alcator C-Mod Tokamak," Phys. Plasmas **23**, 120703 (2016).

[14]P. Manz, T. Happel, U. Stroth, T. Eich, and D. Silvagni, "Physical mechanism behind and access to the I-mode confinement regime in tokamaks," Nucl. Fusion **60**, 096011 (2020).

[15]A. White, P. Phillips, D. Whyte, A. Hubbard, C. Sung, J. Hughes, A. Dominguez, J. Terry, and I. Cziegler, "Electron temperature fluctuations associated with the weakly coherent mode in the edge of I-mode plasmas," Nucl. Fusion **51**, 113005 (2011).

[16]S. Espinosa and P. J. Catto, "Theoretical explanation of I-mode impurity removal and energy confinement," Plasma Phys. Controlled Fusion **60**, 094001 (2018).

[17]I. Cziegler, P. H. Diamond, N. Fedorczak, P. Manz, G. R. Tynan, M. Xu, R. M. Churchill, A. E. Hubbard, B. Lipschultz, J. M. Sierchio, J. L. Terry, and C. Theiler, "Fluctuating zonal flows in the I-mode regime in Alcator C-Mod," Phys. Plasmas **20**, 055904 (2013).

[18]P. Manz, P. Lauber, V. E. Nikolaeva, T. Happel, F. Ryter, G. Birkenmeier, A. Bogomolov, G. D. Conway, M. E. Manso, M. Maraschek, D. Prisiazhniuk, and E. Viezzer, "Geodesic oscillations and the weakly coherent mode in the I-mode of ASDEX Upgrade," Nucl. Fusion **55**, 83004 (2015).

[19]A. Liu, X. Zou, M. Han, T. Wang, C. Zhou, M. Wang, Y. Duan, G. Verdoolaege, J. Dong, Z. Wang, F. Xi, J. Xie, G. Zhuang, W. Ding, S. Zhang, Y. Liu, H. Liu, L. Wang, Y. Li, Y. Wang, B. Lv, G. Hu, Q. Zhang, S. Wang, H. Zhao, C. Qu, Z. Liu, Z. Liu, J. Zhang, J. Ji, X. Zhong, T. Lan, H. Li, W. Mao, and W. Liu, "Experimental identification of edge temperature ring oscillation and alternating turbulence transitions near the pedestal top for sustaining stationary I-mode," Nucl. Fusion **60**, 126016 (2020).

[20]X. Feng, A. Liu, C. Zhou, Z. Liu, M. Wang, G. Zhuang, X. Zou, T. Wang, Y. Zhang, J. Xie, H. Liu, T. Zhang, Y. Liu, Y. Duan, L. Hu, G. Hu, D. Kong, S. Wang, H. Zhao, Y. Li, L. Shao, T. Xia, W. Ding, T. Lan, H. Li, W. Mao, W. Liu, X. Gao, J. Li, S. Zhang, X. Zhang, Z. Liu, C. Qu, S. Zhang, J. Zhang, J. Ji, H. Fan, and X. Zhong, "I-mode investigation on the experimental advanced superconducting tokamak," Nucl. Fusion **59**, 096025 (2019).

[21]P. Manz, G. S. Xu, B. N. Wan, H. Q. Wang, H. Y. Guo, I. Cziegler, N. Fedorczak, C. Holland, S. H. Müller, S. C. Thakur, M. Xu, K. Miki, P. H. Diamond, and G. R. Tynan, "Zonal flow triggers the L–H transition in the experimental advanced superconducting tokamak," Phys. Plasmas **19**, 072311 (2012).

[22]A. J. Creely, S. J. Freethy, W. M. Burke, G. D. Conway, R. Leccacorvi, W. C. Parkin, D. R. Terry, and A. E. White, "Correlation electron cyclotron emission diagnostic and improved calculation of turbulent temperature fluctuation levels on ASDEX Upgrade," Rev. Sci. Instrum. **89**, 53503 (2018).

[23]M. Griener, E. Wolfrum, M. Cavedon, R. Dux, V. Rohde, M. Sochor, J. M. M. Burgos, O. Schmitz, and U. Stroth, "Helium line ratio spectroscopy for high spatiotemporal resolution plasma edge profile measurements at ASDEX Upgrade," Rev. Sci. Instrum. **89**, 10D102 (2018).

[24]M. Griener, J. M. M. Burgos, M. Cavedon, G. Birkenmeier, R. Dux, B. Kurzan, O. Schmitz, B. Sieglin, U. Stroth, E. Viezzer, and E. Wolfrum, "Qualification and implementation of line ratio spectroscopy on helium as plasma edge diagnostic at ASDEX Upgrade," Plasma Phys. Controlled Fusion **60**, 025008 (2018).

[25]W. McCarthy, B. LaBombard, A. Hubbard, J. Terry, A. Kuang, D. Brunner, and J. Hughes, in 63rd Annual Meeting of the APS Division of Plasma Physics, 2021.

[26]J. Candy, E. A. Belli, and R. V. Bravenec, "A high-accuracy Eulerian gyrokinetic solver for collisional plasmas," J. Comput. Phys. **324**, 73–93 (2016).

[27]R. M. McDermott, A. Lebschy, B. Geiger, C. Bruhn, M. Cavedon, M. Dunne, R. Dux, R. Fischer, A. Kappatou, T. Pütterich, and E. Viezzer, "Extensions to the

charge exchange recombination spectroscopy diagnostic suite at ASDEX Upgrade," Rev. Sci. Instrum. **88**, 073508 (2017).

[28] ITER Physics Expert Group on Confinement and Transport, ITER Physics Expert Group on Confinement Modelling and Database, and ITER Physics Basis Editors, "Chapter 2: Plasma confinement and transport," Nucl. Fusion **39**, 2175–2249 (1999).

[29] R. McDermott, C. Angioni, G. Conway, R. Dux, E. Fable, R. Fischer, T. Pütterich, F. Ryter, and E. Viezzer, "Core intrinsic rotation behaviour in ASDEX Upgrade Ohmic L-mode plasmas," Nucl. Fusion **54**, 043009 (2014).

[30] R. Fischer, A. Dinklage, and E. Pasch, "Bayesian modelling of fusion diagnostics," Plasma Phys. Controlled Fusion **45**, 1095–1111 (2003).

[31] G. D. Conway, J. Schirmer, S. Klenge, W. Suttrop, E. Holzhauer, and ASDEX Upgrade Team, "Plasma rotation profile measurements using Doppler reflectometry," Plasma Phys. Controlled Fusion **46**, 951–970 (2004).

[32] T. Happel, A. B. Navarro, G. D. Conway, C. Angioni, M. Bernert, M. Dunne, E. Fable, B. Geiger, T. Görler, F. Jenko, R. M. McDermott, F. Ryter, and U. Stroth, "Core turbulence behavior moving from ion-temperature-gradient regime towards trapped-electron-mode regime in the ASDEX Upgrade tokamak and comparison with gyrokinetic simulation," Phys. Plasmas **22**, 032503 (2015).

[33] A. E. Hubbard, B. A. Carreras, R. L. Boivin, J. W. Hughes, E. S. Marmar, D. Mossessian, and S. J. Wukitch, "Variation of edge gradients with heat flux across L–H and H–L transitions in Alcator C-Mod," Plasma Phys. Controlled Fusion **44**, A359 (2002).

[34] S. J. Freethy, T. Görler, A. J. Creely, G. D. Conway, S. S. Denk, T. Happel, C. Koenen, P. Hennequin, and A. E. White, "Validation of gyrokinetic simulations with measurements of electron temperature fluctuations and density-temperature phase angles on ASDEX Upgrade," Phys. Plasmas **25**, 055903 (2018).

[35] T. D. Rempel, R. F. Gandy, and A. J. Wootton, "Density fluctuation effects on electron cyclotron emission correlation measurements in optically gray plasmas," Rev. Sci. Instrum. **65**, 2044–2048 (1994).

[36] C. Theiler, J. L. Terry, E. Edlund, I. Cziegler, R. M. Churchill, J. W. Hughes, B. LaBombard, and T. Golfinopoulos, "Radial localization of edge modes in Alcator C-Mod pedestals using optical diagnostics," Plasma Phys. Controlled Fusion **59**, 025016 (2017).

[37] A. E. White, W. A. Peebles, T. L. Rhodes, C. H. Holland, G. Wang, L. Schmitz, T. A. Carter, J. C. Hillesheim, E. J. Doyle, L. Zeng, G. R. McKee, G. M. Staebler, R. E. Waltz, J. C. Deboo, C. C. Petty, and K. H. Burrell, "Measurements of the cross-phase angle between density and electron temperature fluctuations and comparison with gyrokinetic simulations," Phys. Plasmas **17**, 056103 (2010).

[38] J. M. Beall, Y. C. Kim, and E. J. Powers, "Estimation of wavenumber and frequency spectra using fixed probe pairs," J. Appl. Phys. **53**, 3933–3940 (1982).

[39] D. Silvagni, J. L. Terry, W. McCarthy, A. E. Hubbard, T. Eich, M. Faitsch, L. Gil, T. Golfinopoulos, G. Grenfell, M. Griener, T. Happel, J. W. Hughes, U. Stroth, and E. Viezzer, "I-mode pedestal relaxation events in the Alcator C-Mod and ASDEX Upgrade tokamaks," Nucl. Fusion **62**, 036004 (2022).

[40] K. Stimmel, A. B. Navarro, T. Happel, D. Told, T. Görler, E. Wolfrum, J. P. M. Collar, R. Fischer, P. A. Schneider, and F. Jenko, "Gyrokinetic investigation of the ASDEX Upgrade I-mode pedestal," Phys. Plasmas **26**, 122504 (2019).

[41] W. McCarthy "The Low Frequency Edge Oscillation in Alcator C-Mod and ASDEX Upgrade I-Mode," Ph.D. Thesis (Massachusetts Institute of Technology Cambridge, MA, 2022).

[42] G. Conway, A. Smolyakov, and T. Ido, "Geodesic acoustic modes in magnetic confinement devices," Nucl. Fusion **62**, 013001 (2022).

[43] L. Frassinetti, M. Beurskens, S. Saarelma, J. Boom, E. Delabie, J. Flanagan, M. Kempenaars, C. Giroud, P. Lomas, C. Meneses, C. Maggi, S. Menmuir, I. Nunes, F. Rimini, E. Stefanikova, H. Urano, and G. Verdoolaege, "Global and pedestal confinement and pedestal structure in dimensionless collisionality scans of low-triangularity H-mode plasmas in JET-ILW," Nucl. Fusion **57**, 016012 (2017).

[44] F. Ryter, C. Angioni, G. Tardini, G. Birkenmeier, P. David, M. Dunne, R. Fischer, T. Pütterich, J. Schweinzer, J. Stober, T. A. U. Team, and T. E. M. Team, "The upgraded ASDEX Upgrade contribution to the ITPA confinement database: Description and analysis," Nucl. Fusion **61**, 046030 (2021).

[45] P. Yushmanov, T. Takizuka, K. Riedel, O. Kardaun, J. Cordey, S. Kaye, and D. Post, "Scalings for tokamak energy confinement," Nucl. Fusion **30**, 1999–2006 (1990).

[46] F. Ryter, C. Angioni, M. Dunne, R. Fischer, B. Kurzan, A. Lebschy, R. McDermott, W. Suttrop, G. Tardini, E. Viezzer, and M. Willensdorfer, "Heat transport driven by the ion temperature gradient and electron temperature gradient instabilities in ASDEX Upgrade H-modes," Nucl. Fusion **59**, 096052 (2019).

[47] A. White, M. Barnes, A. Dominguez, M. Greenwald, N. Howard, A. Hubbard, J. Hughes, D. Mikkelsen, F. Parra, M. Reinke, C. Sung, J. Walk, and D. Whyte, "Reduction of core turbulence in I-mode plasmas in Alcator C-Mod," Nucl. Fusion **54**, 083019 (2014).